International Journal of Nanomedicine

Dovepress
open access to scientific and medical research

Open Access Full Text Article

ORIGINAL RESEARCH

Topical Delivery of ROS-Responsive Methotrexate Prodrug Nanoassemblies by a Dissolvable Microneedle Patch for Psoriasis Therapy

Yong Zhou[1,*], Lei Yang[1,*], Yifu Lyu[1,*], Di Wu[1], Ying Zhu[1], Jingjing Li[1], Dabo Jiang[1], Xiaofei Xin[1], Lifang Yin[1–4]

[1]Department of Pharmaceutics, China Pharmaceutical University, Nanjing, People's Republic of China; [2]NMPA Key Laboratory for Research and Evaluation of Pharmaceutical Preparations and Excipients, China, Nanjing, People's Republic of China; [3]Key Laboratory of Drug Quality Control and Pharmacovigilance, China Pharmaceutical University, Nanjing, People's Republic of China; [4]State Key Laboratory of Natural Medicine, China Pharmaceutical University, Nanjing, People's Republic of China

*These authors contributed equally to this work

Correspondence: Lifang Yin; Xiaofei Xin, Department of Pharmaceutics, China Pharmaceutical University, Nanjing, People's Republic of China, Tel +86 (025)83271018, Email lifangyin@cpu.edu.cn; xxin@cpu.edu.cn

Purpose: Oxidative stress, nuclear factor kappa-light-chain-enhancer of activated B cells (NF-κB) and adenosine signaling are factors associated with psoriatic inflammation. Topical delivery of methotrexate (MTX) has become an option to overcome the side effects caused by systemic therapy in psoriasis, leading to the suppression of NF-κB activation through boosting adenosine release. However, thickened psoriatic skin is the primary restriction against local drug delivery.

Methods: In this study, a ROS responsive MTX prodrug (MTX-TK-HA) was synthesized with the feature of CD44 mediated active targeting to hyperproliferative keratinocytes. MTX prodrug and PLA-mPEG were formulated by nano-precipitation method to develop the MTX-TK-HA/PLA-mPEG nanoassemblies. To achieve painless transdermal delivery, a dissolving microneedle was applied for direct loading of these nanoassemblies by micromolding technique. The particle size, zeta potential, ROS-responsiveness, permeability, and mechanical strength of nanoassemblies and microneedle arrays were determined, respectively. Then, MTT assay, immunoblot analysis, ELISA assay, flow cytometry, and histological staining were utilized to thoroughly evaluate the efficacy of nanoassemblies-loaded microneedles in an imiquimod-induced psoriatic mouse model.

Results: Nanoassemblies-loaded microneedle arrays were capable of significantly penetrating imiquimod-induced psoriatic epidermis in mice. The efficient topical delivery of these nanoassemblies was achieved by potent mechanical strength and hyaluronic acid as the dissolvable matrix for microneedle arrays. CD44-mediated endocytosis enabled the intracellular uptake of nanoassemblies in keratinocytes, and methotrexate was released from MTX-TK-HA with ROS stimuli, followed by suppressing the proliferation of epidermal cells via NF-κB pathway blockade.

Conclusion: In a psoriatic mouse model, nanoassemblies loaded microneedle arrays relieve inflammatory skin disorders via regulation of adenosine and NF-κB signaling. Our study offered a rational design for the transdermal delivery of hydrophobic agents and defined an effective therapeutic option for psoriasis treatment.

Keywords: psoriasis, ROS-responsiveness, microneedle, topical delivery, methotrexate

Introduction

Psoriasis is a chronic auto-inflammatory skin disease followed by prolonged action of oxidative stress, hyperproliferative keratinocytes, and inflamed skin with scaly patches.[1,2] Excessive oxidative stress in psoriatic skin lesions associates with proinflammatory cytokine production via the intracellular kappa-light-chain-enhancer of activated B cells (NF-κB) and mitogen-activated protein kinase signaling (MAPK) signaling pathway.[3] Due to these features, keratinocytes undergo aberrant proliferation and transduce exogenous environmental stimuli for the initiation and perpetuation of cutaneous

Received: 26 October 2022
Accepted: 1 February 2023
Published: 18 February 2023

inflammation.[4,5] Both topical and systemic retinoids, vitamin D and ciclosporin, are utilized in psoriasis treatment.[6] However, concomitant severe side effects including increased risk of coronary heart disease, toxicity and cancer are associated with retinoids and immune drug-based therapies.[7] Regulation of adenosine release is a promising therapeutic strategy for psoriasis patients.[8,9]

Methotrexate (MTX) with modulation of adenosine signaling, anti-proliferative and anti-inflammatory functions, is the first systemic drug of choice for moderate-to-severe psoriatic patients with few side effects but short half-life of 3–10 h.[10,11] Keratinocytes from lesional epidermis exhibited overall 2.9-fold increase of CD44 expression in psoriasis, compared to nonlesional epidermis, which could serve as the active target for nanocarriers.[12,13] For localized psoriatic plaques, keratinocyte-specific targeting of MTX has the potential to elevate the extracellular levels of adenosine by inhibiting 5-aminoimidazole-4-carboxamide ribonucleotide (AICAR) transformylase and disrupt the interplay between skin cells and lymphocytes linked by NF-κB signaling for psoriasis patients.[14,15] Apart from that, hyperproliferative keratinocytes produce excessive amounts of reactive oxygen species (ROS) in the skin lesions of psoriasis patients, leading to the generation of ROS-sensitive materials with controlled and smart release profile.[16,17] However, transdermal delivery of MTX is limited by the poor cutaneous absorption and insufficient passive diffusion through the thick skin.[18] Although medical nanotechnology has provided nanodrug-based topical therapies to improve drug bioavailability and efficacy, nanoparticles around 100–200 nm mainly require chemical enhancers, iontophoresis, thermal ablation and sonophoresis to penetrate the overlying stratum corneum.[19–21]

Nanodrug-loaded dissolving microneedles enable high encapsulation efficiency and precise drug dose with uniform three-dimensional channel distribution.[22] Apart from that, fabrication of dissolving microneedles with biocompatible carbohydrates like hyaluronic acid (HA) or cellulose warrants the invasion ability of microneedles and persistence of therapeutic agents, which address the concerns for direct loading of nanoparticles into dissolving microneedles.[23] To topically arrest keratinocyte hyperproliferation in psoriasis, it is still desired to develop specific-targeting delivery system for druggable targets, especially avoiding phagocytic clearance in skin with greater reactive oxygen levels and lower pH value.[24]

Considering oxidative stress and CD44 overexpression in inflamed psoriatic lesions and epidermal keratinocytes, we utilized the ROS-responsive linker thioketal and HA for oxidative stress-dependent and active targeting delivery of MTX (MTX-TK-HA) to keratinocytes (Scheme 1). Then, poly(lactic acid)-methoxy poly(ethylene glycol) (PLA-mPEG) was synthesized to form nanoassemblies with MTX-TK-HA by nanoprecipitation method. To achieve transcutaneous administration, we further loaded the nanoassemblies into a dissolvable microneedle patch. The matrix content of microneedle was made from HA with molecular weight of 8–12kDa and 100–200kDa to improve the stiffness of microneedle array for reliable insertion in psoriatic skin. Subsequently, the mounting of dissoluble MNs tips was performed by casting the insoluble polystyrene to form a backing layer. After transdermal administration, nanoassemblies filled in microneedle were delivered when exposed to interstitial fluid, followed by internalization through CD44-mediated endocytosis. Afterward, the MTX was released from MTX-TK-HA and exerted its anti-inflammatory actions through the inhibition of NF-κB pathway. Moreover, the competitive inhibition of dihydrofolate reductase led to the repressed hyperproliferation of keratinocytes. We demonstrate that this dissolvable patch integrated with MTX-TK-HA /PLA-mPEG nanoassemblies with ROS-responsive mechanism displayed rapid responsiveness and alleviated the psoriasis-like dermatitis via the blocking of NF-κB pathway.

Materials and Methods

Materials

Methotrexate (MTX, purity ≥99%), hyaluronic acid (HA, 8–12 kDa), hyaluronic acid (HA, 100–200 kDa), 1-hydroxypyrrolidine-2,5-dione (NHS, purity ≥98%) and cysteamine hydrochloride were purchased from Bide Pharmatech Ltd. (Shanghai, China). 4M hydrogen chloride solution in 1,4-dioxane was purchased from Infinity Scientific Co. Ltd. (Beijing, China). 1-(3-dimethylaminopropyl)-3-ethylcarbodiimide hydrochloride (EDCI), 4-dimethylaminopyridine (DMAP), polylactic acid (PLA, 5000 Da), 3-(4,5-dimethylthiazol-2-yl)-2,5-diphenyltetrazolium bromide (MTT) and fluorescein isothiocyanate (FITC) were obtained from Sigma-Aldrich Co. Ltd. (St. Louis, MO, USA). Dialysis tubing

(500–1000 Da, 3500 Da) was purchased from Merck Chemicals Shanghai Co., Ltd (Shanghai, China). HaCaT cell line and fetal bovine serum (FBS) were purchased from Nanjing KeyGEN Biotech Co., Ltd. (Nanjing, China). DMEM medium, trypsin, and penicillin–streptomycin solution were purchased from Fcmacs Biotechnology Co., Ltd. (Nanjing, China). DAPI and Annexin V-FITC/PI staining kit were obtained from the Beyotime Institute of Biotechnology (Shanghai, China).

Cell Culture

HaCaT cells were cultured in Dulbecco's modified Eagle's medium (DMEM) supplemented with 10% FBS, penicillin (100U/mL), and streptomycin (100μg/mL). The cells were incubated in a 100% humidified atmosphere at 37°C with 5% CO_2.

Synthesis of Amphiphilic Prodrug MTX-TK-HA and Amphiphilic Polymer PLA-mPEG

Step 1: Synthesis of ROS-responsive MTX-TK-HA: We synthesized MTX-TK-HA using three following steps: Firstly, cysteamine hydrochloride was reacted with anhydrous acetone in the presence of hydrogen chloride. Then, the reaction was kept in an ice bath for 10 min under vigorous stirring and transferred to room temperature for 12h. The crude TK-NH_2 was filtered and purified by recrystallization. Secondly, MTX-TK was synthesized via amination of MTX with TK-NH_2 using EDCI coupling reaction in the presence of NHS in DMSO. The crude MTX-TK was collected by precipitation and purified by fast silica gel column chromatography. Lastly, the intermediate MTX-TK was reacted with HA (6kDa) in the presence of EDCI and NHS in formamide as the solvent for 48 h. The crude MTX-TK-HA was collected and dialyzed (MWCO=0.5–1kDa) in deionized water for 12 h and lyophilized to obtain MTX-TK-HA. The lyophilization protocol was carried out in a freezing step at −55°C for 4 h, an annealing step at −10°C for 5 h, and a final freezing step at −55°C for 3 h, with the vacuum degree controlled within 15Pa-30Pa.

Step 2: Synthesis of non-responsive MTX-HA: MTX was reacted with HA (6kDa) in the presence of EDCI and DMAP in formamide as the solvent for 48 h. The crude MTX-HA was collected and dialyzed (MWCO=3kDa) in deionized water for 24 h and lyophilized to obtain MTX-HA.

Step 3: Synthesis of PLA-mPEG: PLA-COOH was obtained through the reaction of PLA-OH and succinic anhydride in the presence of DMAP in dichloromethane. After 48 h, the product was collected and purified by recrystallization. Then, PLA-COOH was reacted with mPEG-NH_2 by EDCI/NHS coupling system in dimethyl sulfoxide. The mixture was stirred under nitrogen for 48 h at room temperature and atmospheric pressure and then dialyzed (MWCO=3.5kDa) against hydrochloric acid aqueous solution (0.01M) for 24 h to remove excessive mPEG, followed by dialysis in deionized water for purification and lyophilization to obtain PLA-mPEG.

Preparation and Characterization of MTX-TK-HA/PLA-mPEG Nanoassemblies

MTX-TK-HA/PLA-mPEG nanoassemblies (ROS-responsive nanoassemblies) were prepared with the nano precipitation method as we previously reported.[25] Briefly, 50μL of PLA-mPEG (100 mg/mL in dioxane) solution was added to 1mL of MTX-TK-HA solution (3 mg/mL in PBS) under vigorously stirring. Subsequently, the organic solvent was removed by rotary evaporation. The evaporation system was maintained at a pressure of 500 mm Hg, and the rotation was at a speed of 50 rpm in the water bath of 37 °C. MTX-HA/PLA-mPEG nanoassemblies (Non-responsive nanoassemblies) and the fluorescent labeled nanoassemblies were prepared in the same way by utilizing MTX-HA, MTX-TK-HA-FITC and MTX-TK-HA-Cy5.5, named as Non-res nanoassemblies, FITC-nanoassemblies and Cy5.5-nanoassemblies, respectively. Both FITC and Cy5.5 were covalently conjugated on MTX-TK-HA. The particle size and zeta potential of nanoassemblies were measured with DLS Particle Analyzer (Malvern Panalytical, UK). Then, the critical micelle concentration (CMC) of MTX-TK-HA/PLA-mPEG was determined through the change of fluorescence intensity using pyrene as a fluorescent probe with a microplate reader (Shanpu Limited Company Co., Ltd., Shanghai, China). Briefly, micelles were prepared with an aqueous solution of pyrene of 6.0×10^{-7}mol/L and then the solution was diluted to various concentrations from 284μg/mL to 0.277μg/mL with a constant pyrene concentration of 6.0×10^{-7}mol/L. After incubation at room temperature for 15 h in dark, the samples were transferred to a 96-well black plate with opaque bottom, and the absorbance of pyrene was determined using a microplate reader. The fluorescence intensity ratio (I336/I334) was used to plot against concentration converted to log values.[26]

Preparation and Characterization of Dissolvable Microneedle Patch

Microneedles in this study were fabricated using a polydimethylsiloxane mold from Weixin Pharmaceutical Technology Co., Ltd (Zhejiang, China). Microneedle mold had a 340μm×340μm quadrangular base with rectangular pyramid-shape tapering to a height of 960μm. The microneedle patches were arranged in a 20×20 array with a 310μm tip-to-tip spacing. The matrix material of microneedles was composed of HA with molecular weight of 10kDa and 100kDa. The different mass ratios of those two molecular weights at 3:1, 1:1 and 1:3 were tested to optimize the stiffness and dissolution of microneedle, respectively. 200μL of nanoassemblies and 0.2mL of 10% HA solution were mixed and deposited by pipette onto mold surface. The mold was then placed under vacuum at 30°C for 60 min, followed by centrifuging at 2000 g for 5 min to enable the mixture into the microneedle cavities. The process was repeated until the mixture was dried. Subsequently, a supporting substrate consisting of 20% (w/v) polystyrene in dioxane was gently applied to the molds surface by casting method. After drying in the 37 °C oven for another 12 h, the microneedle patch was carefully detached from the mold and stored in a desiccator. The mechanical properties of the microneedle patch were measured using a texture analyzer (CT3 4500, Brookfield, US). Moreover, the penetration and retention of the microneedle patches were also tested in 1% agarose gel and mouse back skin, respectively. The ex vivo release of MTX from microneedle patch was conducted in stretched porcine skin and the release profile of MTX was determined by the high-performance liquid chromatography at different time points. Franz diffusion cell approach (Shanghai Kaikai Trade Co., Ltd., Shanghai, China) was further applied to verify the MTX release profile from microneedle patch.

In vitro Cytotoxicity and Intracellular Trafficking Process of MTX-TK-HA/PLA-mPEG

The cytotoxicity of the micelles was evaluated using 3-[4,5-dimethylthiazol-2-yl]-2,5 diphenyl tetrazolium bromide (MTT) assay as previously described. HaCaT cells of 3000 per well were seeded in 96-well plate in DMEM medium and incubated for 12h. The cells were treated with MTX, MTX-TK and MTX-TK-HA with the concentration ranging from 15μM to 250μM. After 48 h treatment, 20μL of MTT solution at 5mg/mL was added to each well for another 4 h incubation. The cell culture media were then carefully removed and replaced with 150μL DMSO to dissolve the formazan crystals. The cell viability was measured by a microplate reader (Shanpu Co., Ltd., Shanghai, China) at a wavelength of 492 nm.

Intracellular trafficking of nanoassemblies was examined in HaCaT cells. HaCaT cells of 1×10^5 per dish were seeded in confocal imaging dishes and cultured in 2 mL of DMEM medium containing 10% FBS for 12 h. Then, FITC-nanoassemblies were incubated with HaCaT cells at 37°C with 5% CO_2 in serum-free media for 1 h, 4 h and 6 h, respectively. Afterward, cells were rinsed three times with PBS and stained with DAPI to visualize the nucleus. The cells were imaged by a FV3000 confocal laser scanning microscopy (CLSM, Olympus, Tokyo, Japan).

Western Blot Analysis

Total proteins from HaCaT cells and skin tissues were used for Western blot analysis. Target proteins were probed with the primary antibodies: NF-κB p65 (1:1000, #8242, Cell Signaling Technology, MA, USA), IL-6 (1:1000, 66146-1-Ig, Proteintech, Hubei, China), and β-actin (1:500, sc-47778, Santa Cruz Biotechnology, TX, USA). Matching horseradish peroxidase (HRP) conjugated secondary antibodies were used to analyze the protein levels. The bands were imaged with an automatic chemiluminescence image analysis system (Tanon 5200, Shanghai, China) and normalized to β-actin.

In vivo Biodistribution and Efficacy Study

All the experimental animals were purchased from Nanjing Junke Bioengineering Co., Ltd. (Nanjing, China). All animal studies were performed in accordance with the protocol (#2022-03-002) approved by the institutional animal care and use committee (IACUC) of China Pharmaceutical University. The psoriasis-like mouse model was developed by daily topical application of 62.5mg dose of IMQ cream (Sichuan Med Shine Pharmaceutical Co., Ltd, Sichuan, China). After 1 week, microneedles integrated with free Cy5.5 and Cy5.5-nanoassemblies were transcutaneous treated at a fixed Cy5.5 dose of 1 mg/kg. The in vivo and ex vivo images at 0 h, 4 h, and 24 h were observed by IVIS® Spectrum in vivo imaging system (PerkinElmer, USA).

For therapeutic study, healthy female Balb/c mice (4–5 weeks) were used as control. Psoriasis-like Balb/c mice were randomly divided into five groups for IMQ model (IMQ+PBS), blank microneedle patch (IMQ+Blank MNs), microneedle patch with free MTX (Free MTX-MNs), microneedle patch with Non-res nanoassemblies (Non-res Nano-MNs) and microneedle patch with ROS-responsive nanoassemblies (Nano-MNs), respectively. The microneedle patch was applied 4h after the administration of IMQ cream every two days (days 2, 4 and 6). The dose of MTX was 1mg/kg. Psoriasiform skin inflammation induced by symptoms like erythema and scale was recorded and scored according to the clinical psoriasis area and severity index (PASI) every day for each mouse. Induration, desquamation, and erythema were scored independently on a scale between 0 and 4: 0, none; 1, slight; 2, moderate; 3, marked; 4, very marked. The cumulative score of erythema, scaling, and thickening served as a measure of the severity of inflammation. After 7 days, Western blot analysis and hematoxylin–eosin (H&E) staining were performed to assess the efficacy of microneedle patch with nanoassemblies.

Statistical Analysis

All data are shown as means ± standard deviations (SD). Statistical analysis was performed using one-way ANOVA. Significant differences between different groups were indicated by $*p < 0.05$, $**p < 0.01$ and $***p < 0.001$, respectively. $p < 0.05$ was considered statistically significant.

Results

Preparation and Characterization of ROS-Responsive Nanoassemblies

We first synthesized a HA conjugated ROS-responsive MTX prodrug (MTX-TK-HA) by utilizing thioketal (TK) as the linker by amide condensation reaction (Figure 1A and S4A).[1] H nuclear magnetic resonance (NMR) of TK-NH_2, MTX-TK, MTX-TK-HA, MTX-HA, PLA-COOH and PLA-mPEG was shown in Figures S1-S6. The characteristic signal of protons (a) was at 1.5 parts per million (ppm) for TK and signals assignable to MTX were at 8.58, 8.12, 6.85 and 6.62 ppm (q, p, k and j), indicating a ratio of 2:1 between TK and MTX in final product of MTX-TK (Figure S2). The degree of substitution, defined as the number of grafted MTX-TK per HA, was determined by comparing the integrated peak area of protons q, n, k and i of MTX-TK versus that of the Region A protons of HA at 2.90 to 3.90ppm, which was calculated to be 0.0375 (Figure S3). Likewise, the degree of substitution was calculated to be 0.1483 for MTX-HA (Figure S4B). MTX-TK-HA and MTX-HA obtained in the present study were considered to have sufficient repeating units to interact with CD44.[27,28] For PLA-COOH, the characteristic peaks were at 1.54–1.62 (a), 3.80 (b) and 5.19 (c) ppm (Figure S5). For PLA-mPEG, the characteristic peaks at 1.63 ppm (a) and 3.68, 3.82 and 5.22 ppm (e, f, g) matched well for mPEG and PLA, respectively (Figure S6). Then, MTX-TK-HA was encapsulated in nanoassemblies by facile co-precipitation with PLA-mPEG to obtain spherical particles with an average diameter of 118.2nm, a PDI of 0.182 and a ζ-potential of 0.019mV (Figure 1C, D and 2A). As shown in Figure 2B, CMC for MTX-TK-HA/PLA-mPEG nanoassemblies was 3.17μg/mL, which marked the lower limit of these nanoassemblies to ensure the integrity of micelles. In addition, nanoassemblies appeared to be stable in PBS buffers with pH values of 5.0, 6.0 and 7.4 (Figure 2C-E). The size distributions were not altered with the concentrations of nanoassemblies (Figure 2F).

Enhanced CD44-Mediated Endocytosis and Inhibited NF-κB Signaling Pathway by Nanoassemblies in Keratinocytes

To better understand the keratinocyte association and uptake properties of MTX-TK-HA/PLA-mPEG nanoassemblies, the experiment was performed in HaCaT cells, which was observed by confocal microscopy at 1h, 4h and 6h. Confocal imaging showed presence of FITC-nanoassemblies was in a positive punctate pattern in the cytoplasm at 4 h when compared to free FITC solution, indicating CD44-mediated internalization was involved in the cellular uptake of nanoassemblies (Figure 3A).[27,28] Then, the hemolysis assay was used to evaluate the hemolytic behaviors of nanoassemblies on mouse red blood cells. Compared to positive control of polyethyleneimine (PEI), ROS-responsive nanoassemblies did not display a visible hemolytic effect at different concentrations. No significant difference was observed when the concentration of MTX-TK-HA ranged from 0.5 to 3.0mg/mL (Figure 3B and C). With abundant accumulation in keratinocytes and superior biocompatibility, we applied an in vitro imiquimod (IMQ) induced HaCaT cell model with

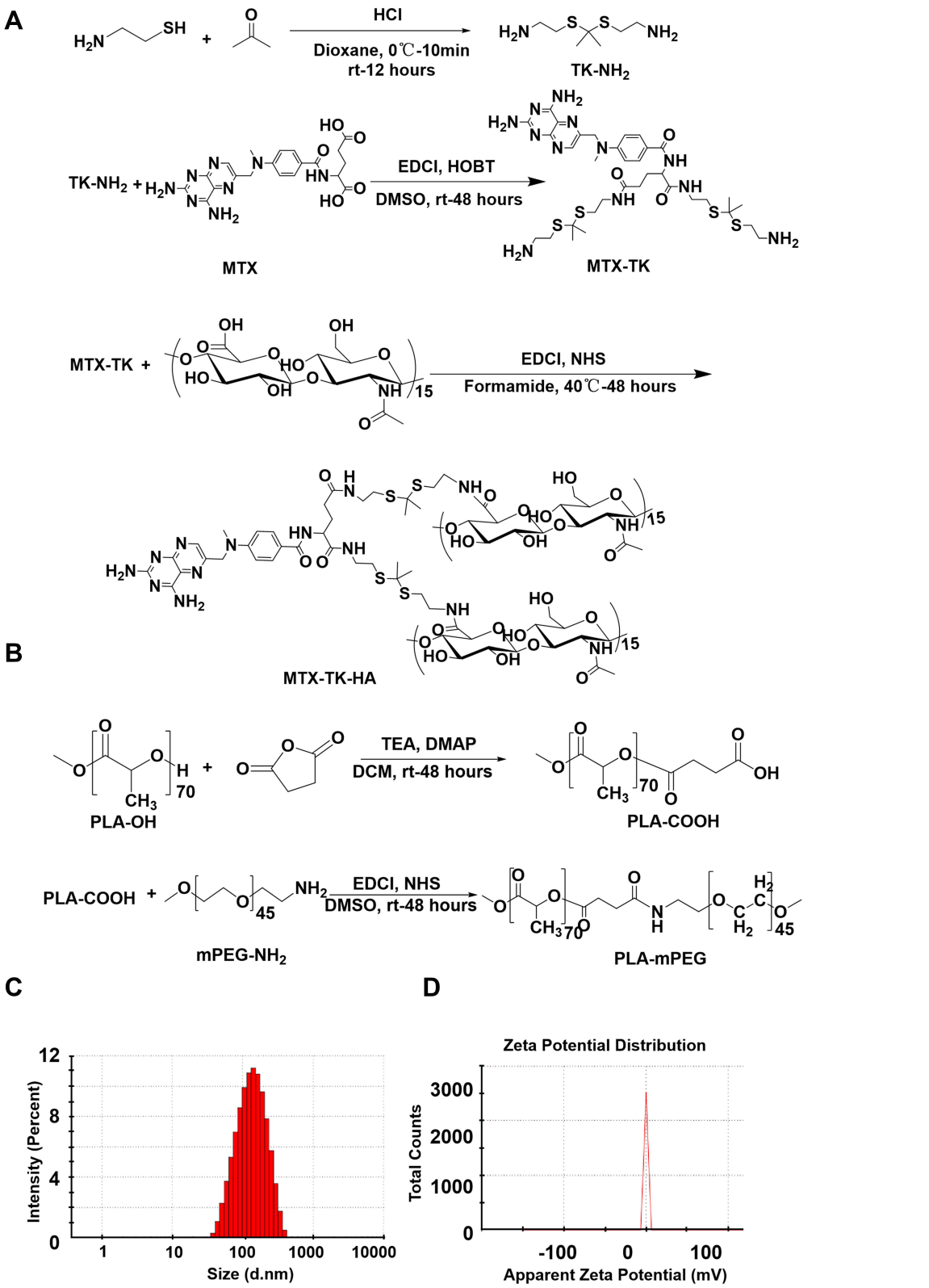

Figure 1 Preparation and characterization of MTX-TK-HA/PLA-mPEG nanoassemblies. Synthesis scheme for (**A**) ROS-responsive HA-conjugated methotrexate prodrug (MTX-TK-HA) and (**B**) PLA-mPEG, respectively. (**C**) Particle size and (**D**) zeta-potential distribution of MTX-TK-HA/PLA-mPEG nanoassemblies.

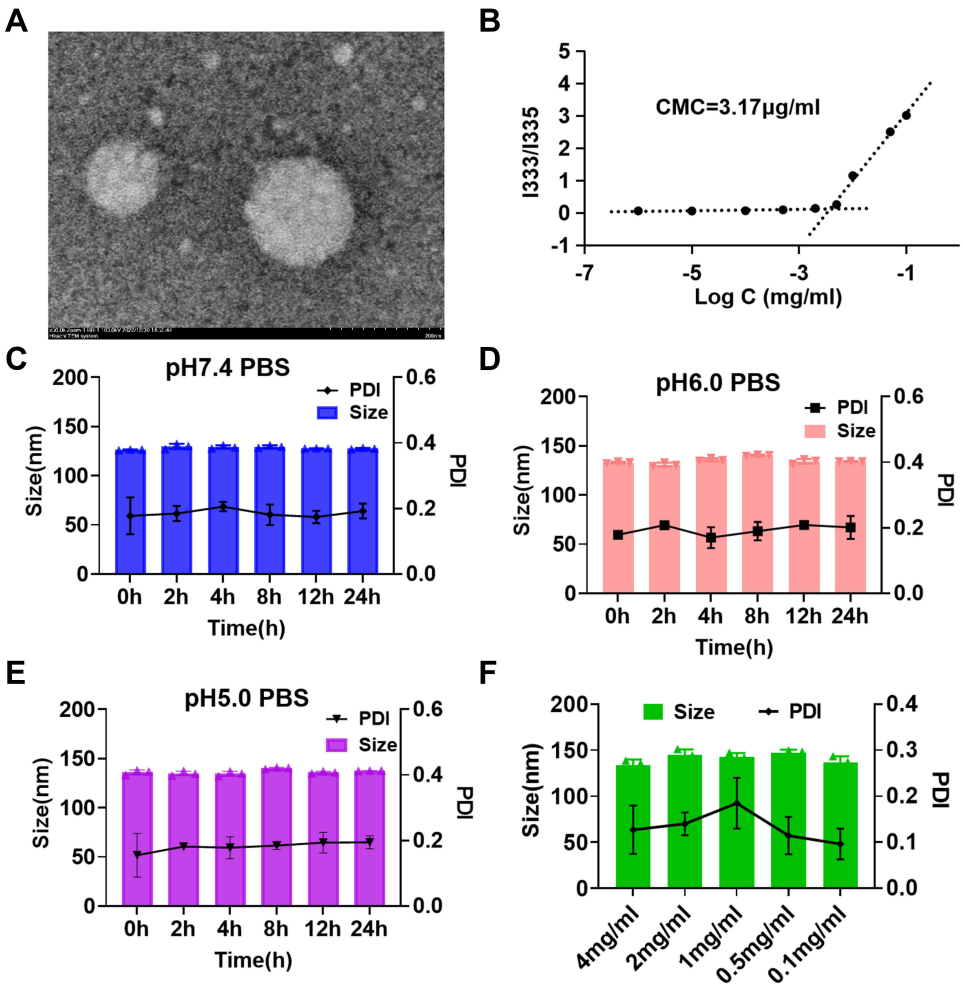

Figure 2 (**A**) TEM image of MTX-TK-HA/PLA-mPEG nanoassemblies. Scale bar 200 nm. (**B**) Critical micelle concentration of MTX-TK-HA/PLA-mPEG nanoassemblies. (**C-E**) Stability of nanoassemblies in PBS buffers with pH of 7.4, 6.0, 5.0, respectively. (**F**) Size distributions of MTX-TK-HA/PLA-mPEG nanoassemblies in different concentrations.

inflammatory response to evaluate whether the modification of HA affected the MTX efficacy. The Western blotting bands showed significant enhancement of NF-κB and IL-6 expression levels in HaCaT cells when subjected to 25μg/mL of IMQ for 24h, whereas NF-κB and IL-6 levels were reduced by MTX-TK-HA/PLA-mPEG nanoassemblies in IMQ stimulated HaCaT cells, which was better than Non-responsive nanoassemblies (Figure 3D-F). The downregulation of NF-κB and IL-6 levels has the potential to hinder the cell viability and cell division of HaCaT cells. By performing MTT assay, MTX, MTX-TK and MTX-TK-HA at 500μM caused 37.9%, 19.2% and 22.6% cytotoxicity to HaCaT cells, respectively (Figure 4A and B). Accordingly, redistribution of HaCaT cells across the cell cycle phases resulted in significant cell cycle arrest at S phase and further enhanced the MTX efficacy in psoriasis (Figure 4C and D). These data also indicate the sustained-release profile of MTX-TK and MTX-TK-HA, compared to the free MTX solution.

Dissolvable Microneedles Loaded with Nanoassemblies Achieved Topical Delivery

Next, nanodrug-based dissolvable microneedles were fabricated utilizing a micromolding technique for painless transdermal administration (Figure 5A). Photographs of nanoassemblies integrated microneedles with trypan blue and nanoassemblies confirmed the formation of microneedle arrays, respectively (Figure 5B). HA was selected as the main matrix for microneedles because it is highly biocompatible with a suitable mechanical property, as we ascertained in the measurement of mechanical strength. Microneedles required a force of 0.109, 0.089 and 0.041N/needle with the ratio of HA-10kDa and HA-100kDa at 1/3, 1/1 and 3/1 for failure to occur, respectively (Figure 5C). The trypan blue staining test

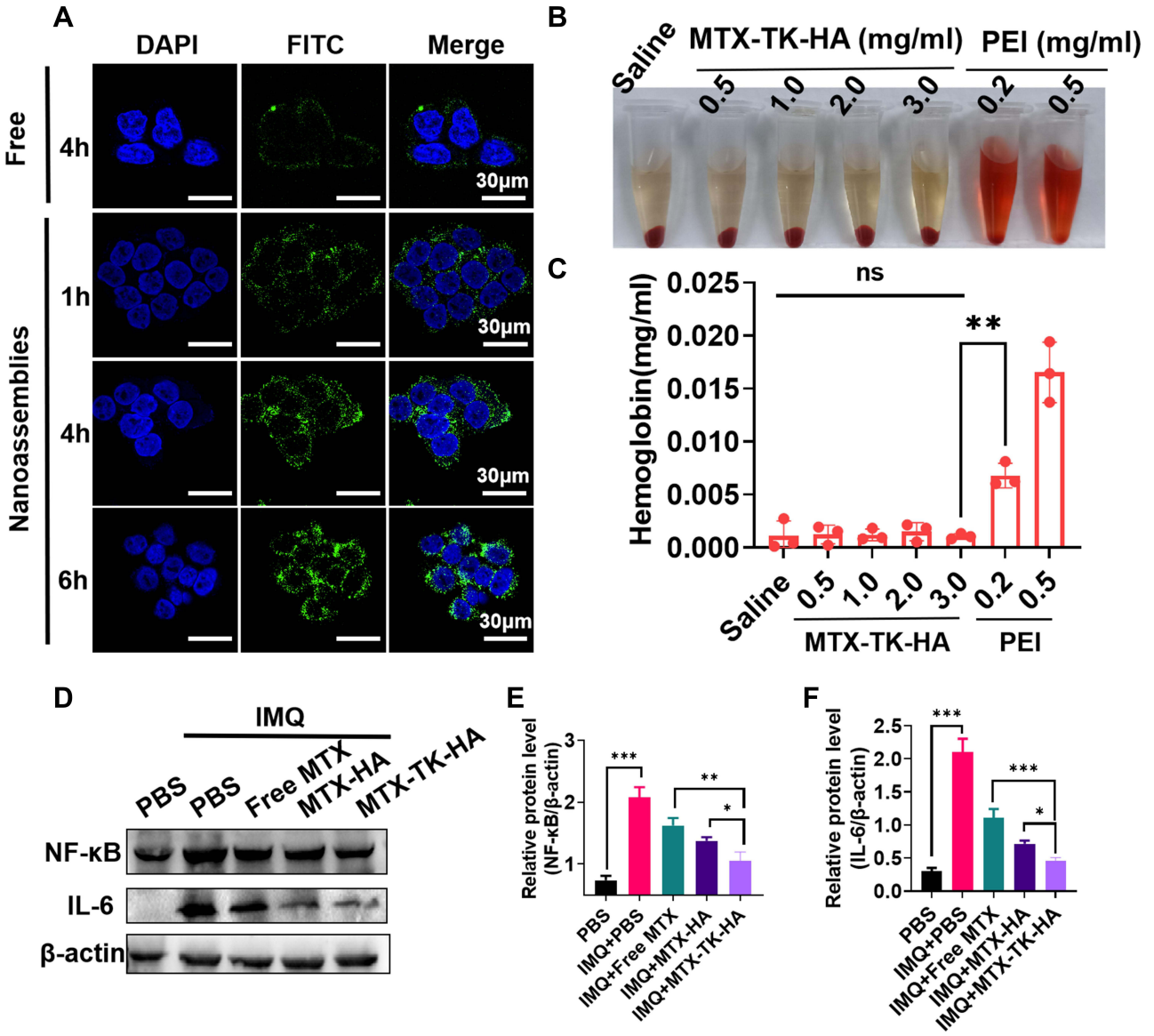

Figure 3 (**A**) CLSM images of HaCaT cells incubated with FITC-nanoassemblies for 1h, 4 h and 6h, respectively. Nucleus was stained with DAPI (blue). Scale bars are 30μm. (**B** and **C**) Hemolysis assay of MTX-TK-HA/PLA-mPEG nanoassemblies. PEI was used as the positive control. (**D-F**) Western blot analysis of NF-κB and IL-6 expression in IMQ induced HaCaT cells. Results are presented as the mean ± SD (n=3). *P<0.05, **P<0.01 and ***P<0.001, One-Way ANOVA test.

on the 1% agarose gel and mouse skin further validated this finding (Figure 5D). These data demonstrate sufficient strength for skin insertion. The fluorescence image of FITC/Cy5.5-nanoassemblies loaded microneedles suggested that nanoassemblies were distributed mostly inside the needle tips with pyramid shape (Figure 5E). To optimize the ratio of HA-10kDa and HA-100kDa for rapid dissolving profile of microneedles, microneedle arrays were inserted in porcine skin for different periods of time. The microneedle started to dissolve within 1 min and entirely dissolved after 15 min for the ratio of HA-10kDa and HA-100kDa at 3/1 and 1/1 (Figure 5F). Therefore, it is rational to choose the ratio of HA-10kDa and HA-100kDa at 1/1 to achieve potent mechanical strength and efficient delivery of MTX-TK-HA/PLA-mPEG nanoassemblies for overcoming the skin epidermal barrier in psoriasis. Then, the permeation profile of FITC-nanoassemblies through the mouse skin was carried out by vertical Franz diffusion cell. After applying microneedle arrays to the mouse skin, 30.6% of FITC-MTX-TK-HA were detected at 15 min and the cumulative release percentage reached 91.1% within 120 min (Figure 5G), demonstrating nanoassemblies integrated microneedles was able to penetrate the cuticle layer of skin. We further evaluated the ROS-responsive release capability of nanoassemblies after dissolving

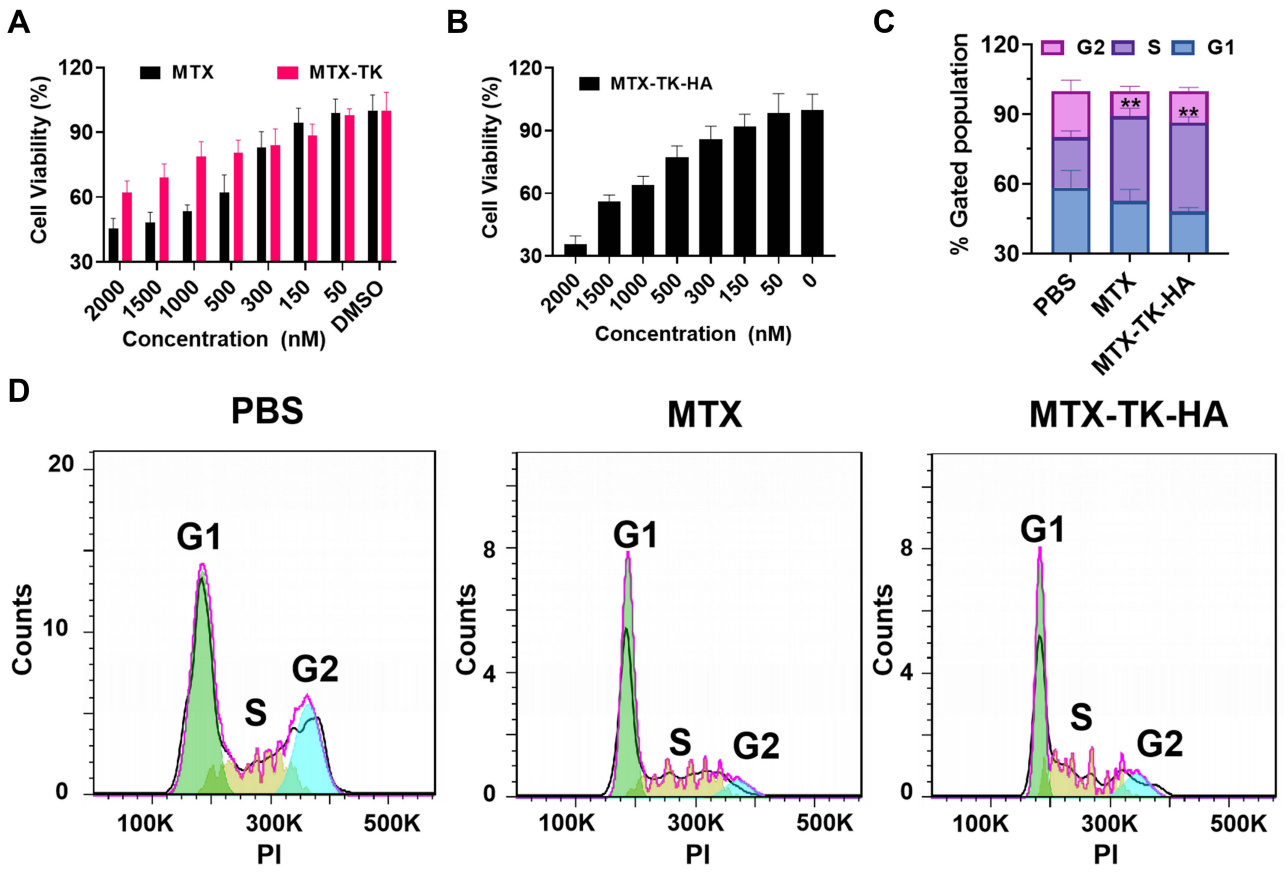

Figure 4 (**A** and **B**) Cell viability of HaCaT cells with the treatment of MTX, MTX-TK and MTX-TK-HA at different doses. (**C** and **D**) Cell cycle study of MTX-TK-HA/PLA-mPEG nanoassemblies compared with free MTX solution. Results are presented as the mean ± SD (n=3). **P<0.01, One-Way ANOVA test.

from microneedle arrays. More than 44.8% of FITC was released within 8h when compared to non-ROS responsive condition (Figure 5H), indicating the ROS-dependent release profile of those nanoassemblies.

Microneedle Arrays Loaded with Nanoassemblies Alleviate Psoriasis-Like Dermatitis

Psoriatic mice were treated with Cy5.5-nanoassemblies integrated microneedle arrays. The distribution of Cy5.5-nanoassemblies in both tissue and organ aspects was visualized by the IVIS® Spectrum in vivo imaging system (PerkinElmer, USA) at different time points after treatment. The free Cy5.5 solution loaded microneedle arrays were used as the control. Compared to free Cy5.5 solution, the fluorescence intensity of Cy5.5-nanoassemblies was strong in the psoriatic skin lesions but absent in the heart, liver, spleen, lung and kidney within 5 h (Figure 6). There was almost no Cy5.5 fluorescent signal observed in the skin lesion at the time point of 24 h, confirming the rapid dissolution of nanoassemblies loaded microneedle in vivo.

We then evaluated the in vivo performance of nanodrug-loaded microneedle-array patches in a psoriasis-like mouse model induced by IMQ cream. The mice were divided into five groups treated with PBS, blank microneedle array patches (blank MNs), free MTX loaded microneedle patch (Free MTX-MNs), Non-res nanoassemblies loaded microneedle patch (Non-res Nano-MNs) and ROS-responsive nanoassemblies loaded microneedle array patches (Nano-MNs) according to the illustration in Figure 7A. The healthy mice were used as the control. During the treatment from day 1 to 3, an obvious body weight loss was observed after the topical application of IMQ cream. The body weight of Nano-MNs group was gradually restored from day 4 (Figure 7B). Splenomegaly was evaluated by the spleen weight and the ratio of spleen weight to body weight in IMQ-induced mice after treatment. Compared to healthy control, topical application of IMQ led to an increased spleen weight and spleen-weight to body-weight ratio (Figure 7C-E). Western blotting results further ascertained IMQ-induced inflammation as shown by the upregulation of NF-κB and IL-6 levels in psoriatic skin

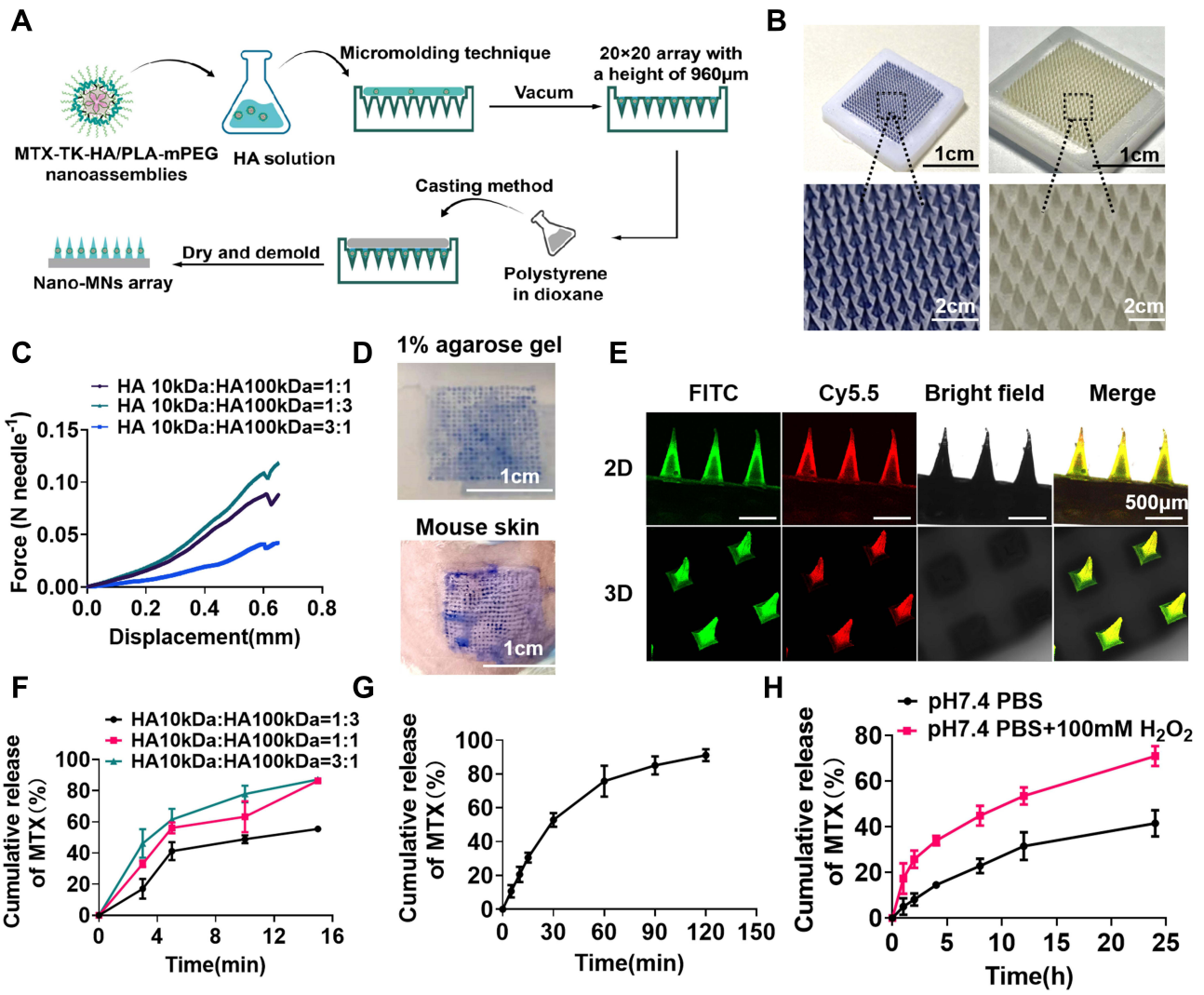

Figure 5 Fabrication and characterization of dissolvable microneedles. (**A**) Illustration of the fabrication process of Nano-MNs using a micromolding technique. (**B**) Representative photographs of Nano-MNs containing trypan blue or nanoassemblies. (**C**) Mechanical strength test for Nano-MNs. (**D**) Photographs of 1% agarose gel and mouse skin after the insertion of trypan blue loaded MNs. (**E**) Fluorescence microscopy imaging of a microneedle patch with FITC/Cy5.5-nanoassemblies. (**F**) In vitro cumulative MTX release from MTX-MNs prepared with HA-10kDa and HA-100kDa at ratios of 1/3, 1/1 and 3/1 in porcine skin, respectively. (**G**) In vitro cumulative release of MTX from Nano-MNs using a Franz diffusion cell approach. (**H**) In vitro ROS responsive release of MTX from the FITC-nanoassemblies. Results are presented as the mean ± SD (n=3).

lesions. NF-κB and IL-6 levels were suppressed 2.33-/2.29-, 2.88-/2.78-, 1.93-/1.98-, 1.33-/1.54-fold after Nano-MNs treatment as compared to PBS, blank MNs, Free MTX-MNs and Non-res Nano-MNs treated mice, respectively (Figure 7F-H). Consistent with the restoration of body weight and spleen weight, the Nano-MNs treatment relieved the overall pro-inflammatory state via boosting the cAMP level by 10.6% and 6.1% (Figure 7I), compared to Free MTX-MNs and Non-res Nano-MNs, which might lead to the elevation of intracellular release of adenosine.

For further justification of psoriasiform inflammation, PASI was determined for different treatment groups in IMQ-induced mouse model. Psoriatic-like animals receiving PBS and blank MNs displayed remarkable skin thickening, scaling and redness from day 3. It was noticeable that Nano-MNs showed an efficient and rapid improvement in psoriatic skin when observed on day 5 (Figure 8A-D and S7). On day 6, Nano-MNs treatment exhibited a significantly different total PASI score from PBS and blank MNs in psoriatic-mouse model, upon applying one-way ANOVA statistical analysis (Figure 8E and F). Blank MNs showed non-significant variation from PBS group during treatment, suggesting good biocompatibility of microneedle array in vivo as verified in the histological analysis for liver and spleen tissues (Figure 8F, 9A and B). Meanwhile, the epidermal thickness was decreased 2.84-, 3.04-, 1.66-, 1.45-fold after Nano-

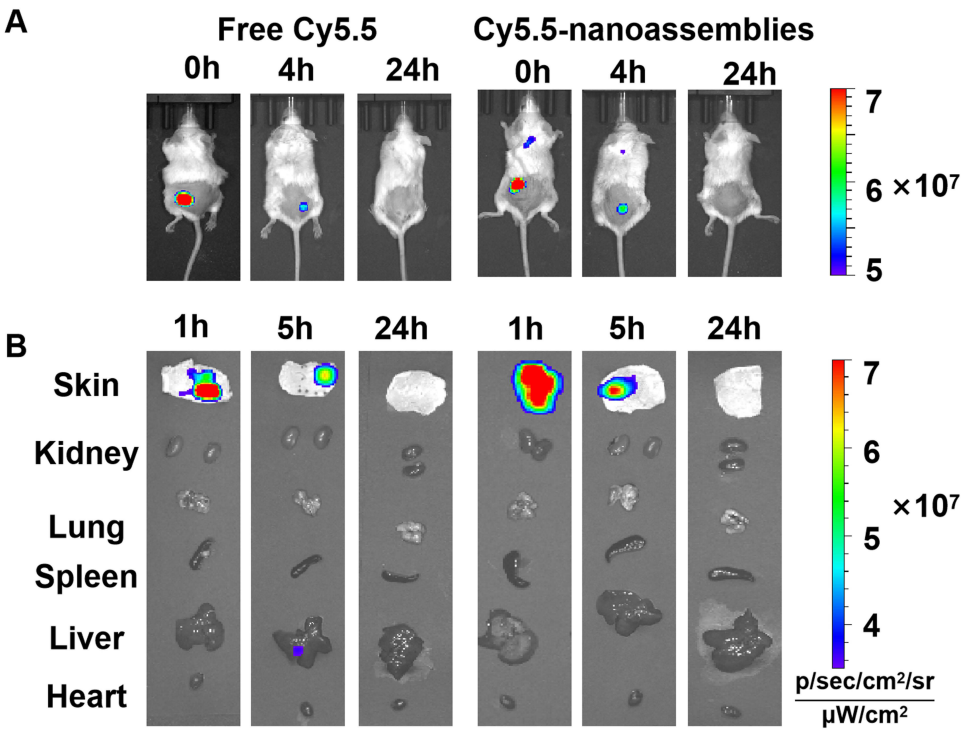

Figure 6 (**A**) In vivo imaging of Cy5.5-nanoassemblies in IMQ-induced psoriasis-like mice after the application of Cy5.5-nanoassemblies loaded microneedles at 0h, 4h and 24h, respectively. (**B**) Ex vivo images of the skin and main organs at 1h, 5h and 24h, respectively.

MNs treatment as compared to PBS, blank MNs, Free MTX-MNs and Non-res Nano-MNs treated mice, respectively (Figure 8G). Correspondingly, H&E staining revealed that psoriasis pathogenesis was altered in the epidermis with the decrease in hyperkeratosis, acanthosis and elongation of rete ridges into the dermis (Figure 9C). These data demonstrate the therapeutic potency of Nano-MNs in the regulation of adenosine and NF-κB signaling to resolve inflammation in psoriasis, with good tolerance, and superior permeability and delivery efficiency with properties of CD44 targeting and ROS responsiveness.

Discussion

In this study, we have developed a ROS-responsive and CD44-active targeting prodrug of MTX, which formed self-assembled nanodrugs with PLA-mPEG (Figures 1 and 2). The size distribution of nanoassemblies was 126.0 to 149.8nm with PDI around 0.1–0.2, with the concentrations ranging from 0.1 to 4 mg/mL (Figure 2E). In our previous reports, we have thoroughly demonstrated that HA with molecular weight of 6kDa, has sufficient CD44-targeting ability by cellular uptake, endocytic pathway inhibitors and receptor saturation test.[27,28] Therefore, the internalization of designed nanoassemblies with MTX-TK-HA in this study was expected to be dominated by CD44-mediated pathway in CD44 highly expressed keratinocytes, as we observed in Figure 3A.

Advantages of the thioketal moiety include its stability to enzymes and acidic or basic environments, resulting in the stability of nanoassemblies in endosomes/lysosomes. It readily cleaved into its non-toxic thiol and acetone products when exposed to pathological levels of ROS in vitro or in vivo.[29] The susceptibility of TK to various ROS includes superoxide (O_2•$^-$), hydrogen peroxide (H_2O_2), hypochlorite (OCl^-), peroxynitrite ($ONOO^-$) and hydroxyl radical (•OH).[30,31] The CD44-targeting and ROS-responsiveness of these nanoassemblies enabled precise delivery of MTX to CD44 over-expressed keratinocytes with adequate stability in local acidic environment of psoriatic lesions (Figures 2C-E and 5H). Compared to non-responsive nanoassemblies, the treatment of MTX-TK-HA/PLA-mPEG nanoassemblies showed 23.1% and 35.6% decrease of NF-κB and IL-6 levels in IMQ-induced HaCaT cells (Figure 3D-F). These results provide sufficient evidence for ROS-responsive release of MTX from MTX-TK-HA/PLA-mPEG nanoassemblies in vitro.

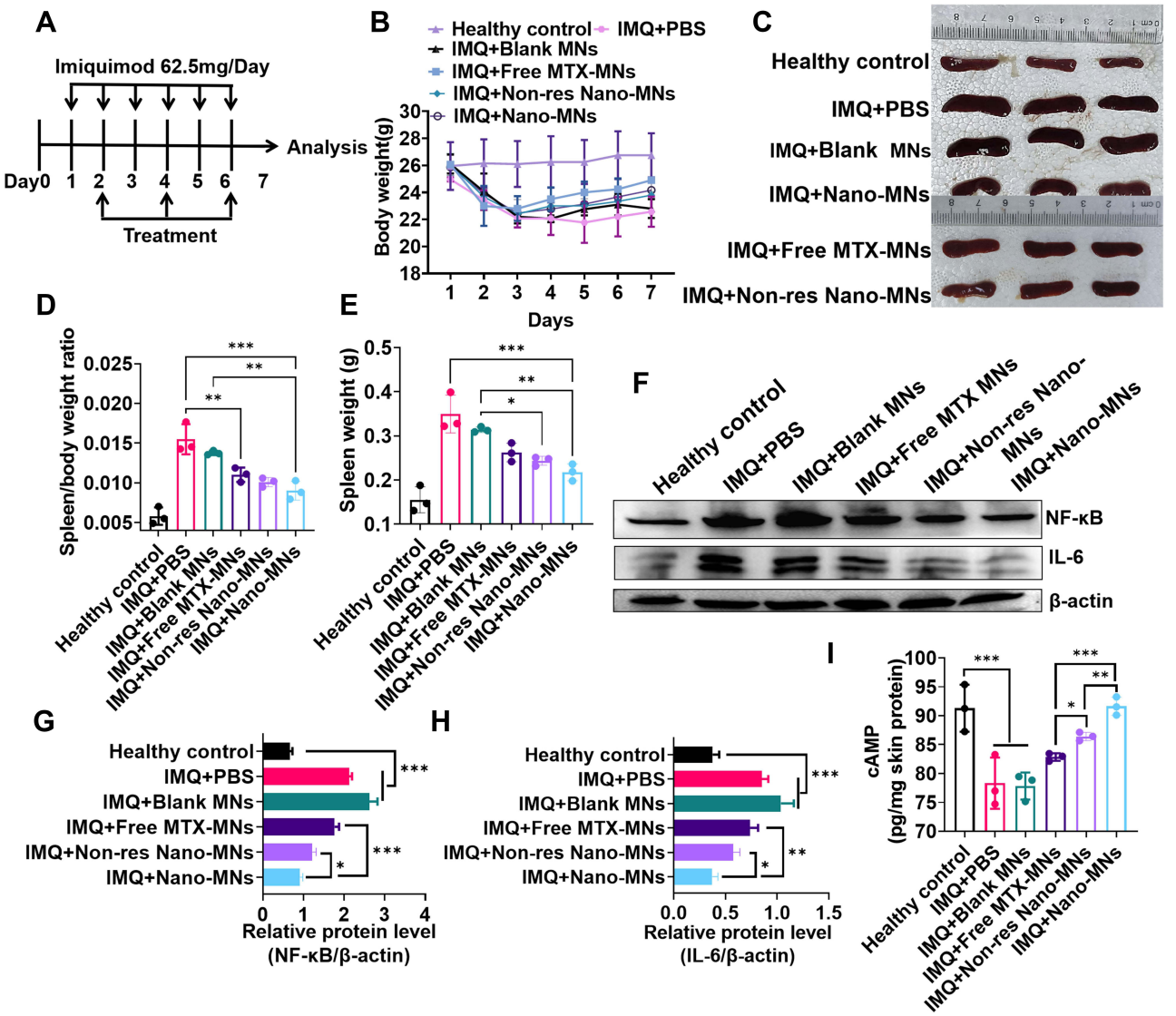

Figure 7 Microneedle arrays loaded with nanoassemblies alleviate the psoriasis-like dermatitis. (**A**) Schematic illustration of Nano-MNs for the psoriasis treatment. (**B**) The alternation of the body weight during treatments. (**C** and **D**) Spleen weight and spleen/body weight ratio of mice at day 7. (**E**) Representative photographs of the isolated spleen at day 7. (**F-H**) Immunoblot analysis of NF-κB and IL-6 expression levels in the inflamed skin homogenates. (**I**) ELISA analysis of cAMP level in the psoriatic skin. *P<0.05, **P<0.01 and ***P<0.001, One-Way ANOVA test.

Due to the biodegradable and mechanical nature of HA, the encapsulation of these nanoassemblies in HA matrix-based microneedle arrays can prevent the leakage of therapeutic nano-agent (Figure 6). The molecular weight of HA has a direct impact on the viscoelasticity and stiffness of microneedle arrays.[23,32] To bear enough mechanical strength for overcoming the physical skin barrier in psoriatic lesions, we fabricated nanoassemblies loaded microneedles with different ratios of HA molecular weight to facilitate the microneedle arrays for penetrating the skin, getting dissolved and releasing of the nano-cargoes (Figure 5F and G). Meanwhile, microneedle length determines the drug loading, strength, depth of penetration, cell targeting and release rates of dissolvable microneedle arrays.[33] Microneedle arrays with needles longer than 600μm were considered to be more effective in penetrating the skin and enhancing drug release. In our study, the needle density of microneedle arrays was calculated to be 123 needles/cm^2, which was less than 2000 needles/cm^2 and might lead to elevated drug flux with long enough needle length.[34] Xu et al embedded UCNPs@mSiO$_2$ in a 10×10 stainless MN array with a tip length of 1000 μm was used as the template, and found robust penetration and cargo release of UCNPs@mSiO$_2$ in mouse dorsal skin for skin disease therapy.[35] Therefore, we selected a microneedle length of 960μm to achieve nanoassemblies loading, robust needle insertion and potent therapeutic response.[33]

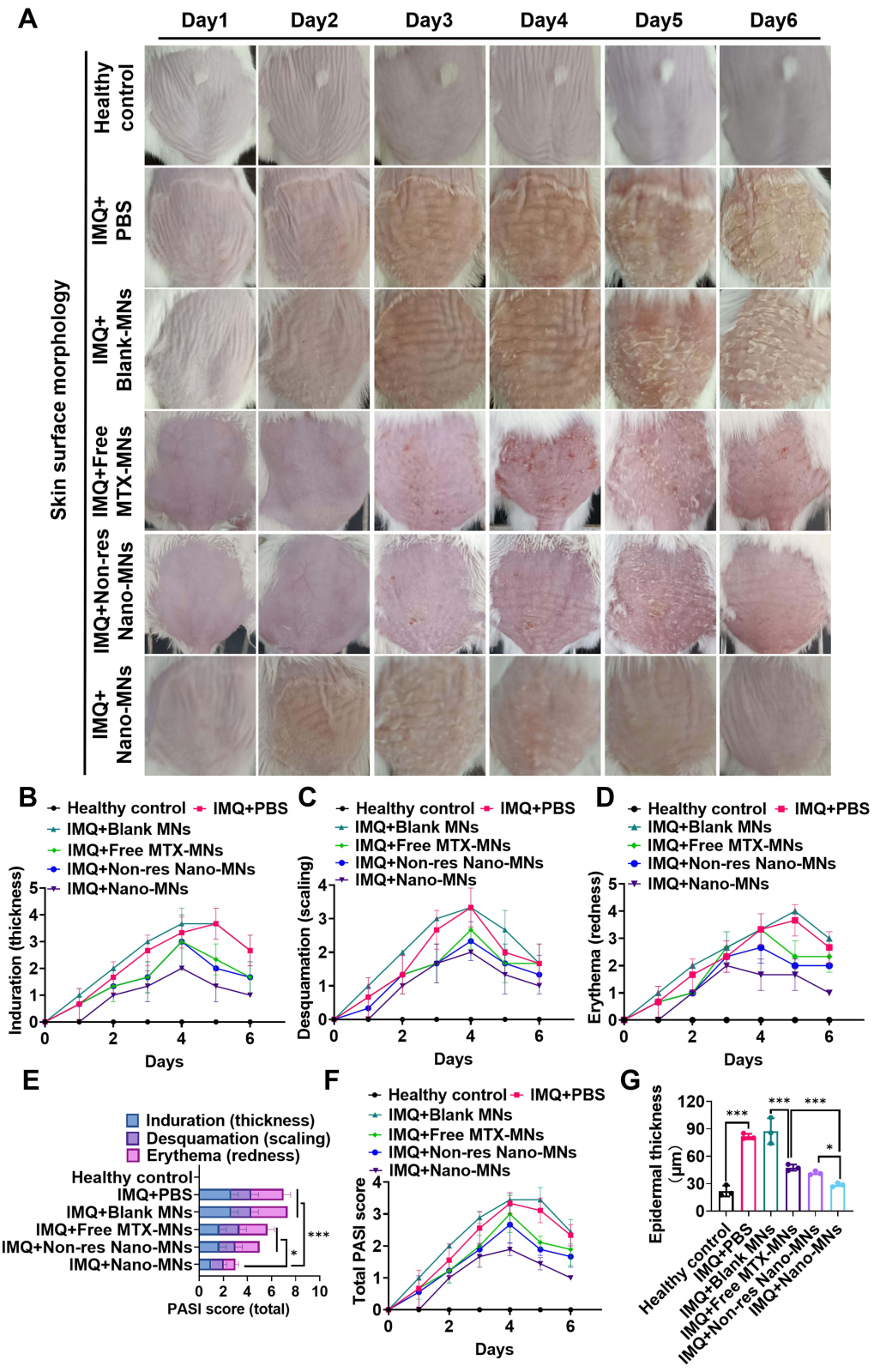

Figure 8 Skin morphology and PASI score in psoriatic mouse model after Nano-MNs treatment. (**A**) The appearance and morphology of skin from day 1 to day 6. Healthy mice were used as the control. (**B-F**) Induration, desquamation, erythema and total PASI scores of the back skin. (**G**) Analysis of the thickness of the epidermal layer of mouse back skin in H&E staining sections. *P<0.05 and ***P<0.001, One-Way ANOVA test.

https://doi.org/10.2147/IJN.S394957 DovePress

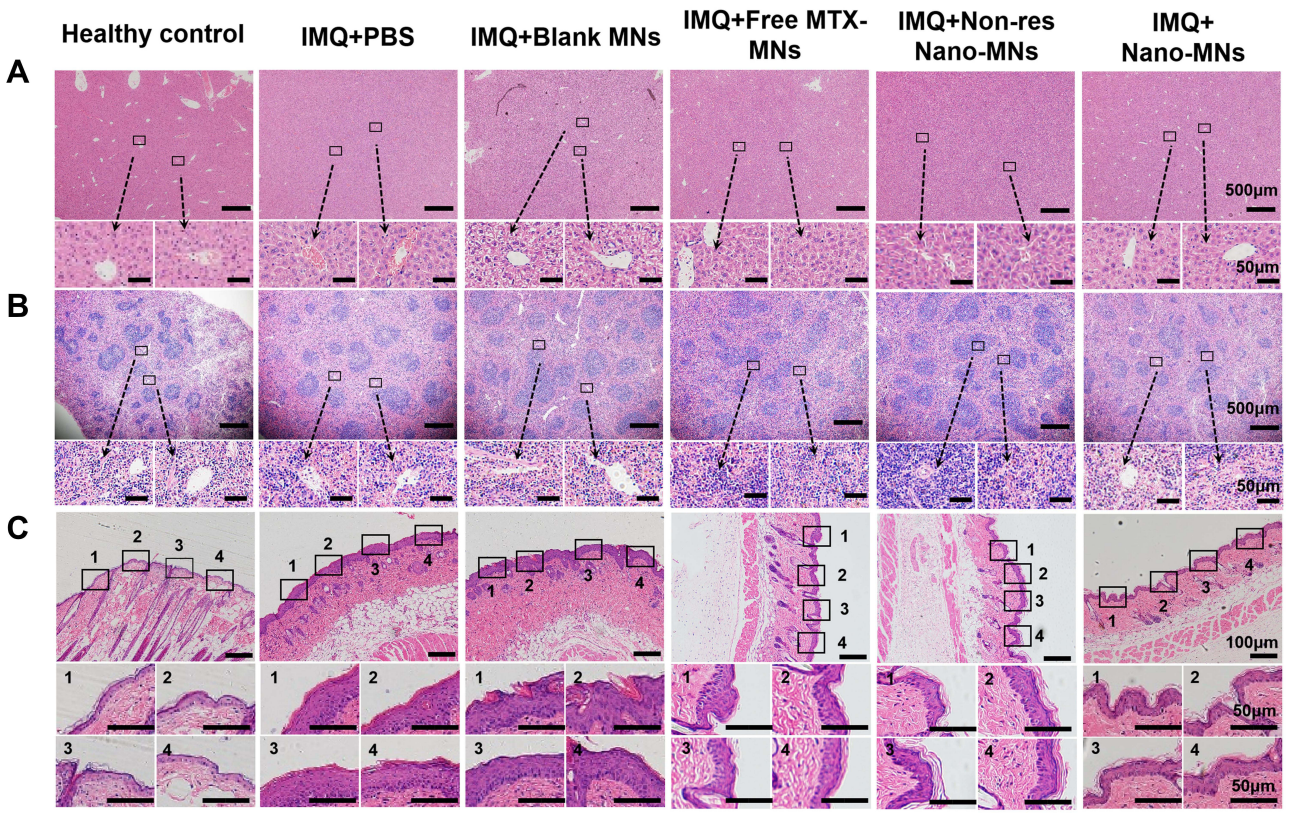

Figure 9 Representative H&E staining of liver (**A**), spleen (**B**) and skin sections (**C**) at day 7. The inset indicates the enlarged views.

Utilizing the in vivo murine psoriasis-like mouse model, we characterized the therapeutic efficacy of MTX-TK-HA/PLA-mPEG nanoassemblies integrated microneedle array. In the IMQ-induced psoriatic mouse model, decrease in body weight was accompanied by a prominent splenomegaly, which was consistent with previous report.[36,37] Importantly, Nano-MNs were well tolerated at the MTX dose of 1mg/kg following topical administration, and no treatment modality has been shown in IMQ-induced psoriatic mouse model, indicating the high in vivo biocompatibility of these microneedle patches. Our in vitro data provided a mechanistic explanation to the efficacy of MTX-TK-HA through cytotoxicity, cell cycle and Western blotting assay (Figures 3D and 4). Consistently, the 7-day topical treatment with MTX prodrug-based nanoassemblies suppressed the proliferation of keratinocytes and acted directly on adenosine and NF-κB signaling to restore local immune homeostasis (Figure 7F-I). Most importantly, we also explored the efficacy of Free MTX-MNs and Non-res Nano-MNs for the in-vivo study, which further ascertained the superior efficacy of Nano-MNs with CD44 targeting and ROS responsiveness (Figures 7–9). Consequently, this established formulation efficiently mitigated the psoriasis development afterward, as we validated with PASI score and H&E staining (Figures 8 and 9C).

Conclusion

In summary, MTX-TK-HA/PLA-mPEG nanoassemblies were designed to achieve CD44-targeting and ROS-responsive release of MTX in hyperproliferative keratinocytes for psoriasis. With robust nanodrug loading and needle insertion of microneedle, these ROS-responsive nanoassemblies loaded dissolving microneedle arrays can further potentially alleviate inflammatory skin disorder in psoriasis via regulation of NF-κB and adenosine signaling. Compared to free MTX-MNs and Non-res Nano-MNs, ROS-responsive nanoassemblies in microneedle exhibited prominent improvement in NF-κB signaling regulation, cAMP restoration, and skin morphology. Furthermore, the concept of this ROS-responsive and ligand-mediated active targeting microneedle arrays can be extended to applications related to ROS-responsive prodrug delivery for treating other diseases.

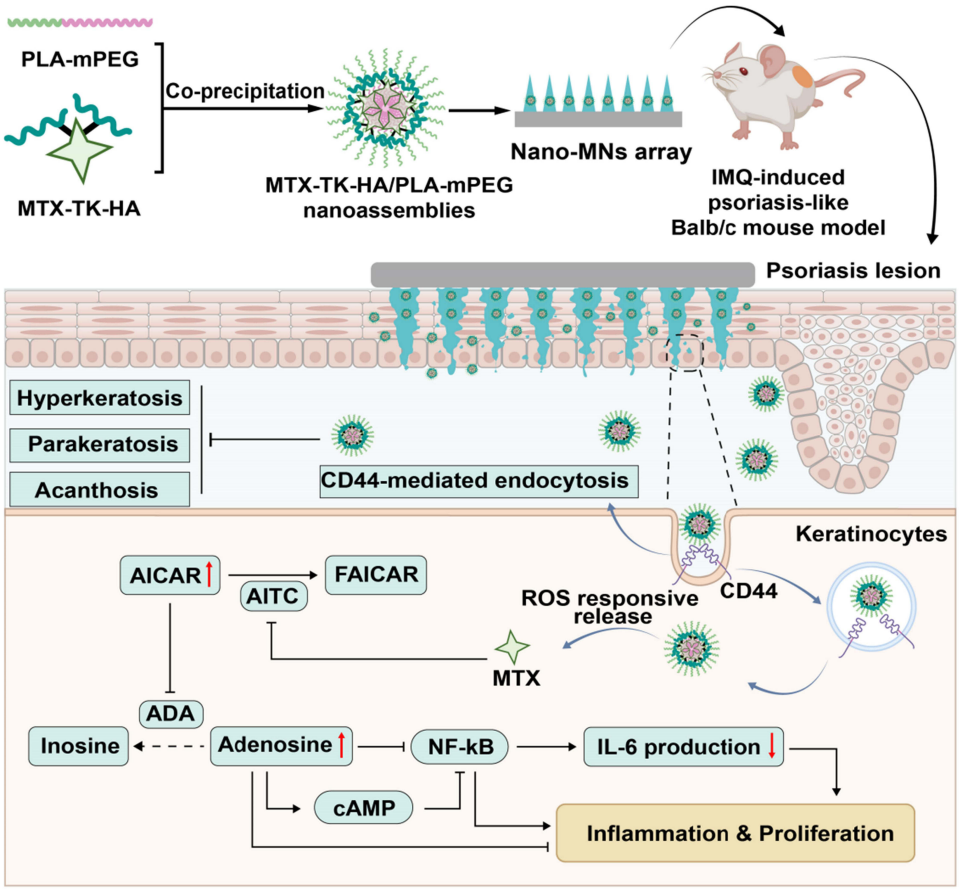

Scheme 1 Illustration of topical delivery of MTX by Nano-MNs array for anti-inflammatory effect in psoriasis treatment. MTX-TK-HA/PLA-mPEG nanoassemblies were prepared by facile co-precipitation, and then loaded in the dissolvable microneedles utilizing a micromolding technique for painless transdermal administration. After applying Nano-MNs to the psoriasis lesion, the nanoassemblies was rapidly released and accumulated in keratinocytes via CD44-mediated endocytosis, followed by ROS-responsive release of MTX to exert anti-inflammation and anti-proliferation effect.

Abbreviations

HA, hyaluronic acid; ROS, reactive oxygen species; TK, thioketal; MTX, methotrexate; MTX-TK, thioketal modified methotrexate; MTX-TK-HA, hyaluronic acid conjugated reactive oxygen species-responsive methotrexate prodrug; Cy5.5, cyanine 5.5; FITC, fluorescein isothiocyanate; FBS, fetal bovine serum; MTX-TK-HA-FITC, fluorescein isothiocyanate modified methotrexate prodrug; MTX-TK-HA-Cy5.5, cyanine 5.5 modified methotrexate prodrug; PLA, polylactic acid; PLA-mPEG, poly(lactic acid)-methoxy poly(ethylene glycol) ; MNs, microneedles; IMQ, imiquimod; MAPK, mitogen-activated protein kinase signaling; NF-κB, the nuclear factor kappa-light-chain-enhancer of activated B cells; AICAR, 5-aminoimidazole-4- carboxamide ribonucleotide; pH, potential of hydrogen; NHS, 1-hydroxypyrrolidine-2,5-dione; DMAP, 4-dimethylaminopyridine; EDCI, 1-(3-dimethylaminopropyl)-3-ethylcarbodiimide hydrochloride; MTT, 3-(4,5-dimethylthiazol-2-yl)-2,5-diphenyltetrazolium bromide; DMEM, Dulbecco's modified Eagle medium; DAPI, 4',6-diamidino-2-phenylindole; PI, propidium iodide; MWCO, molecular weight cut off; PBS, phosphate buffered saline; DLS, dynamic light scattering; CMC, critical micelle concentration; kDa, kilodalton; w/v, weight by volume; DMSO, dimethyl sulfoxide; IL-6, interleukin-6; HRP, horseradish peroxidase; IACUC, institutional animal care and use committee; PASI, psoriasis area and severity index; H&E, hematoxylin-eosin; SD, standard deviations; ANOVA, analysis of variance; NMR, ^{1}H nuclear magnetic resonance; PEI, polyethyleneimine; Blank MNs, blank microneedle array patches; Nano-MNs, nanoassemblies loaded microneedle array patches; cAMP, cyclic adenosine 3′:5′-monophosphate; CLSM, laser scanning confocal microscopy; SD, standard deviation.

Funding

The National Natural Science Foundation of China (81871477) and the Natural Science Foundation of Jiangsu Province (BK20221045) are duly acknowledged for providing financial support for this work.

Disclosure

All authors report no conflicts of interest in this work.

References

1. Ni X, Lai Y. Keratinocyte: a trigger or an executor of psoriasis? *J Leukoc Biol*. 2020;108(2):485–491. doi:10.1002/jlb.5mr0120-439r
2. Lin X, Huang T. Oxidative stress in psoriasis and potential therapeutic use of antioxidants. *Free Radic Res*. 2016;50(6):585–595. doi:10.3109/10715762.2016.1162301
3. Baek J, Lee MG. Oxidative stress and antioxidant strategies in dermatology. *Redox Rep*. 2016;21(4):164–169. doi:10.1179/1351000215y.0000000015
4. Miodovnik M, Koren R, Ziv E, Ravid A. The inflammatory response of keratinocytes and its modulation by vitamin D: the role of MAPK signaling pathways. *J Cell Physiol*. 2012;227(5):2175–2183. doi:10.1002/jcp.22951
5. Bito T, Nishigori C. Impact of reactive oxygen species on keratinocyte signaling pathways. *J Dermatol Sci*. 2012;68(1):3–8. doi:10.1016/j.jdermsci.2012.06.006
6. Ogawa E, Sato Y, Minagawa A, Okuyama R. Pathogenesis of psoriasis and development of treatment. *J Dermatol*. 2018;45(3):264–272. doi:10.1111/1346-8138.14139
7. López-Cano M, Filgaira I, Nolen EG, et al. Optical control of adenosine A(3) receptor function in psoriasis. *Pharmacol Res*. 2021;170:105731. doi:10.1016/j.phrs.2021.105731
8. Merighi S, Borea PA, Varani K, Gessi S. Deregulation of Adenosine Receptors in Psoriatic Epidermis: an Option for Therapeutic Treatment. *J Invest Dermatol*. 2017;137(1):11–13. doi:10.1016/j.jid.2016.08.001
9. Ciruela F, Jacobson KA. Optical Control of Adenosine A(3) Receptor Signaling: towards a Multimodal Phototherapy in Psoriasis? *Front Immunol*. 2022;13:904762. doi:10.3389/fimmu.2022.904762
10. Nedelcu RI, Balaban M, Turcu G, et al. Efficacy of methotrexate as anti-inflammatory and anti-proliferative drug in dermatology: three case reports. *Exp Ther Med*. 2019;18(2):905–910. doi:10.3892/etm.2019.7511
11. Coates LC, Merola JF, Grieb SM, Mease PJ, Callis Duffin K. Methotrexate in Psoriasis and Psoriatic Arthritis. *J Rheumatol Suppl*. 2020;96:31–35. doi:10.3899/jrheum.200124
12. Ekman AK, Bivik Eding C, Rundquist I, Enerbäck C. IL-17 and IL-22 Promote Keratinocyte Stemness in the Germinative Compartment in Psoriasis. *J Invest Dermatol*. 2019;139(7):1564–1573.e8. doi:10.1016/j.jid.2019.01.014
13. Lugović-Mihić L, Novak-Bilić G, Vučić M, Japundžić I, Bukvić I. CD44 expression in human skin: high expression in irritant and allergic contact dermatitis and moderate expression in psoriasis lesions in comparison with healthy controls. *Contact Dermatitis*. 2020;82(5):297–306. doi:10.1111/cod.13463
14. Darwish NF, Tabra SAA, Baiomy NN, Mahmoud HA, Mariah RA, Hablas SA. The implication of adenosine receptor expression in prediction of methotrexate clinical response in Egyptian rheumatoid arthritis patients. *Egyptian Rheumatology Rehabilitation*. 2022;49(1):5. doi:10.1186/s43166-021-00107-9
15. Tsuruta D. NF-kappaB links keratinocytes and lymphocytes in the pathogenesis of psoriasis. *Recent Pat Inflamm Allergy Drug Discov*. 2009;3(1):40–48. doi:10.2174/187221309787158399
16. Hua Y, Chang T, Jiang K, et al. ROS-sensitive calcipotriol nano-micelles prepared by methoxypolyethylene glycol (mPEG) - modified polymer for the treatment of psoriasis. *Drug Deliv*. 2022;29(1):1903–1913. doi:10.1080/10717544.2022.2086944
17. Hu J, Bian Q, Ma X, Xu Y, Gao J. A double-edged sword: ROS related therapies in the treatment of psoriasis. *Asian J Pharm Sci*. 2022;17(6):798–816. doi:10.1016/j.ajps.2022.10.005
18. Aickara D, Bashyam AM, Pichardo RO, Feldman SR. Topical methotrexate in dermatology: a review of the literature. *J Dermatolog Treat*. 2022;33(1):512–517. doi:10.1080/09546634.2020.1770170
19. Li N, Qin Y, Dai D, et al. Transdermal Delivery of Therapeutic Compounds With Nanotechnological Approaches in Psoriasis. *Front Bioeng Biotechnol*. 2021;9:804415. doi:10.3389/fbioe.2021.804415
20. Roberson ED, Bowcock AM. Psoriasis genetics: breaking the barrier. *Trends Genet*. 2010;26(9):415–423. doi:10.1016/j.tig.2010.06.006
21. Li J, Ghatak S, El Masry MS, et al. Topical Lyophilized Targeted Lipid Nanoparticles in the Restoration of Skin Barrier Function following Burn Wound. *Mol Ther*. 2018;26(9):2178–2188. doi:10.1016/j.ymthe.2018.04.021
22. Zhao Y, Zhou Y, Yang D, et al. Intelligent and spatiotemporal drug release based on multifunctional nanoparticle-integrated dissolving microneedle system for synergetic chemo-photothermal therapy to eradicate melanoma. *Acta Biomater*. 2021;135:164–178. doi:10.1016/j.actbio.2021.09.009
23. Bhadale RS, Londhe VY. A systematic review of carbohydrate-based microneedles: current status and future prospects. *J Mater Sci Mater Med*. 2021;32(8):89. doi:10.1007/s10856-021-06559-x
24. Bigliardi PL. Role of Skin pH in Psoriasis. *Curr Probl Dermatol*. 2018;54:108–114. doi:10.1159/000489524
25. Xin X, Kumar V, Lin F, et al. Redox-responsive nanoplatform for codelivery of miR-519c and gemcitabine for pancreatic cancer therapy. *Sci Adv*. 2020;6(46):548. doi:10.1126/sciadv.abd6764
26. Li H, Hu D, Liang F, Huang X, Zhu Q. Influence factors on the critical micelle concentration determination using pyrene as a probe and a simple method of preparing samples. *R Soc Open Sci*. 2020;7(3):192092. doi:10.1098/rsos.192092
27. Xin X, Zhou Y, Li J, Zhang K, Qin C, Yin L. CXCL10-coronated thermosensitive "stealth" liposomes for sequential chemoimmunotherapy in melanoma. *Nanomedicine*. 2022;48:102634. doi:10.1016/j.nano.2022.102634
28. Lv Y, Xu C, Zhao X, et al. Nanoplatform Assembled from a CD44-Targeted Prodrug and Smart Liposomes for Dual Targeting of Tumor Microenvironment and Cancer Cells. *ACS Nano*. 2018;12(2):1519–1536. doi:10.1021/acsnano.7b08051

29. Rinaldi A, Caraffi R, Grazioli MV, et al. Applications of the ROS-Responsive Thioketal Linker for the Production of Smart Nanomedicines. *Polymers*. 2022;14(4):548. doi:10.3390/polym14040687
30. Li J, Ding Z, Li Y, et al. Reactive oxygen species-sensitive thioketal-linked mesoporous silica nanoparticles as drug carrier for effective antibacterial activity. *Mater Des*. 2020;195:109021. doi:10.1016/j.matdes.2020.109021
31. Shim MS, Xia Y. A reactive oxygen species (ROS)-responsive polymer for safe, efficient, and targeted gene delivery in cancer cells. *Angew Chem Int Ed Engl*. 2013;52(27):6926–6929. doi:10.1002/anie.201209633
32. Saha I, Rai VK. Hyaluronic acid based microneedle array: recent applications in drug delivery and cosmetology. *Carbohydr Polym*. 2021;267:118168. doi:10.1016/j.carbpol.2021.118168
33. Makvandi P, Kirkby M, Hutton ARJ, et al. Engineering Microneedle Patches for Improved Penetration: analysis, Skin Models and Factors Affecting Needle Insertion. *Nanomicro Lett*. 2021;13(1):93. doi:10.1007/s40820-021-00611-9
34. Yan G, Warner KS, Zhang J, Sharma S, Gale BK. Evaluation needle length and density of microneedle arrays in the pretreatment of skin for transdermal drug delivery. *Int J Pharm*. 2010;391(1–2):7–12. doi:10.1016/j.ijpharm.2010.02.007
35. Wang M, Han Y, Yu X, et al. Upconversion Nanoparticle Powered Microneedle Patches for Transdermal Delivery of siRNA. *Adv Healthc Mater*. 2020;9(2):e1900635. doi:10.1002/adhm.201900635
36. Thatikonda S, Pooladanda V, Sigalapalli DK, Godugu C. Piperlongumine regulates epigenetic modulation and alleviates psoriasis-like skin inflammation via inhibition of hyperproliferation and inflammation. *Cell Death Dis*. 2020;11(1):21. doi:10.1038/s41419-019-2212-y
37. Zhang J, Yang X, Qiu H, Chen W. Weight loss may be unrelated to dietary intake in the imiquimod-induced plaque psoriasis mice model. *Open Life Sci*. 2020;15(1):79–82. doi:10.1515/biol-2020-0009